

# Fate of surface gaps in magnetic topological insulators

Habib Rostami<sup>1,\*</sup> and Ali G. Moghaddam<sup>2,3,4,†</sup>

<sup>1</sup>*Department of Physics, University of Bath, Claverton Down, Bath BA2 7AY, United Kingdom*

<sup>2</sup>*Department of Physics, Institute for Advanced Studies in Basic Sciences (IASBS), Zanjan 45137-66731, Iran*

<sup>3</sup>*Computational Physics Laboratory, Physics Unit, Faculty of Engineering and Natural Sciences, Tampere University, P.O. Box 692, FI-33014 Tampere, Finland*

<sup>4</sup>*Helsinki Institute of Physics, FI-00014 University of Helsinki, Finland*

(Dated: April 30, 2024)

In magnetic topological insulators, the surface states can exhibit a gap due to the breaking of time-reversal symmetry. Various experiments, while suggesting the existence of the surface gap, have raised questions about its underlying mechanism in the presence of different magnetic orderings. Here, we demonstrate that magnon-mediated electron-electron interactions, whose effects are not limited to the surfaces perpendicular to the magnetic ordering, can significantly influence surface states and their effective gaps. On the surfaces perpendicular to the spin quantization axis, many-body interactions can enhance the band gap to a degree that surpasses the non-interacting scenario. Then, on surfaces parallel to the magnetic ordering, we find that strong magnon-induced fermionic interactions can lead to features resembling a massless-like gap. These remarkable results largely stem from the fact that magnon-mediated interactions exhibit considerable long-range behavior compared to direct Coulomb interactions among electrons, thereby dominating the many-body properties at the surface of magnetic topological insulators.

## INTRODUCTION

The commencement of the new century has coincided with groundbreaking discoveries in condensed matter physics. Notably, the theoretical prediction and experimental realization of various topological phases of matter have revolutionized our understanding of even the most fundamental electronic properties of solids [1–3]. Beyond their fundamental significance, topological materials have proven to be highly promising for advanced technological applications such as nanoelectronics, spintronics, and quantum technologies [4–6]. A quintessential hallmark of three-dimensional topological phases, upon which much of the intriguing physics and potential applications hinge, is the existence of two-dimensional (2D) surface states that offer protection against perturbations, disorder, and imperfections [7–10].

Recently, the discovery of magnetic topological insulators (MTIs), wherein nontrivial topology intersects with magnetic ordering in either antiferromagnetic (AFM) or ferromagnetic (FM) forms, has introduced a new dimension to topological physics that attracted significant attention in the community [11–13]. From a theoretical standpoint, MTIs exhibit exotic phenomena such as the quantum anomalous Hall effect and axion electrodynamics, arising from time-reversal-symmetry (TRS) breaking and a magnetically-induced gap in the surface bands [14–19]. From a practical perspective, MTIs hold promise for applications in spintronics, magnetic memories, and other domains [20–25]. The pursuit of experimental realization of MTIs has met substantial success, with can-

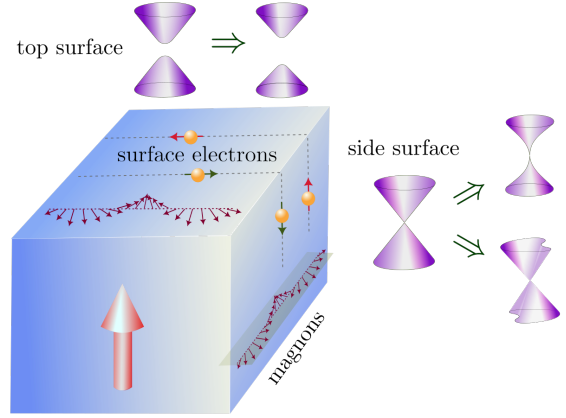


FIG. 1. Schematic illustration of magnon-mediated interactions effects on the spectral properties of topological surface states. The surface states exhibit helical electronic modes, and magnons are represented in two orientations, perpendicular and parallel to the spin quantization axis (depicted by a prominent red arrow). In the absence of interactions, the side surface is expected to remain gapless. However, the top and bottom surfaces, oriented perpendicular to the spin quantization axis, develop a gap if subjected to a finite exchange field  $m_{\perp}$ . Upon considering interaction effects, we observe an increase in the gap amplitude at the top/bottom surfaces, whereas on side surfaces we have significant velocity enhancement. Moreover, certain interaction limits can lead to strong spectral features similar to a massless gap opening.

didate materials such as  $\text{EuSn}_2\text{As}_2$  and  $\text{MnBi}_{2n}\text{Te}_{3n+1}$  families being extensively studied [26–41].

Interestingly, the precise measurement of surface states dispersion and especially the magnetic gap have turned out to be challenging and still under debate from theoretical and experimental perspectives [42–46]. In a standard scenario, while symmetry breaking in magnetically

\* hr745@bath.ac.uk

† agorbantz@iasbs.ac.ir

ordered phases ensures the existence of a surface state Dirac mass gap, it is expected that the gap will vanish above the critical temperature. However, various experiments indicate that the gap persists even beyond the magnetic transition, notably in the case of antiferromagnetic topological insulators (TIs) such as  $\text{MnBi}_2\text{Te}_4$  [28–30]. Conversely, there are other findings in FM compounds or heterostructures, such as  $\text{MnBi}_8\text{Te}_{13}$ , which exhibit substantial consistency with the aforementioned symmetry-breaking framework [47–50].

In this paper, motivated by the ongoing debate in the community and the overlooked interplay between magnetic excitations and electronic properties in these systems [51, 52], we investigate the role of magnons in the surface states of MTIs. Specifically, we demonstrate how magnons can mediate a strong effective electron-electron interaction, giving rise to intriguing many-body effects on the spectral properties of the Dirac surface states, as schematically illustrated in Fig. 1. Interestingly, we find that effective interactions unveil a distinctive momentum dependence characterized by a screening feature, with the effective length scale inversely proportional to the magnon gap. We establish that, whether in the presence or absence of a finite magnon gap, the resulting interacting fermionic model exhibits similarities to disparate models such as Gross-Neveu [53–55] and Hatsugai-Kohmoto [56], which possess short- and long-range interactions, respectively. This observation positions Magnetic Topological Insulators (MTIs) as promising candidates for probing exotic many-body features associated with theoretical models.

Next, we calculate the renormalization effects on the surface states' dispersion induced by magnon-mediated interactions. For surfaces perpendicular to the magnetic ordering, we find an enhancement of the gap caused by the effective interactions which can be comparable and even substantially larger than the non-interacting Dirac gap. In stark contrast, on surfaces parallel to the magnetization, where there is no explicit symmetry-breaking induced Dirac gap, we demonstrate that the matrix form of magnon-electron coupling results in either isotropic or anisotropic velocity renormalization, the latter always accompanied by a tilting effect. Notably, the scenario of isotropic velocity renormalization asymptotically approaches the diverging Fermi velocity renormalization which features similar behavior to *massless gap opening* [57–61], in the limit of gapless magnons. The massless-gapped phase (mostly known in the context of the HK model) resembles the Mott gap induced by electron-electron interaction in the Hubbard model and offers a rich platform to explore unconventional superconductivity based on an exactly solvable Mott insulating normal state [62, 63].

## RESULTS

**Surface electrons coupled to magnons.** In the low-energy limit, the surface states are typically governed by the Dirac Hamiltonian

$$\mathcal{H}_e = \sum_{\mathbf{k}} \psi_{\mathbf{k}}^\dagger (v_F \mathbf{k} \cdot \boldsymbol{\sigma} + \mathbf{m} \cdot \boldsymbol{\sigma}) \psi_{\mathbf{k}}, \quad (1)$$

Here,  $\psi_{\mathbf{k}}^\dagger = (\psi_{\mathbf{k}\uparrow}^\dagger, \psi_{\mathbf{k}\downarrow}^\dagger)$  represents the two-component creation field operator, and  $\psi_{\mathbf{k}}$  is the corresponding annihilation operator for electrons with momentum  $\mathbf{k}$ . The magnetic term  $\mathbf{m} \cdot \boldsymbol{\sigma}$  at each surface with respect to its orientation decomposes into a Dirac gap contribution  $m_\perp \sigma_\perp$  and a momentum shift term  $m_\parallel \sigma_\parallel$ , which can be gauged out for constant uniform magnetization. Therefore, we only need to consider the Dirac gap, caused by the perpendicular component of the magnetization to the considered surface. It is simply  $m_z$  for the top surface in the  $xy$  plane, while it vanishes for the side surfaces in the  $xz$  or  $yz$  plane, as depicted in Fig. 1. The magnetic ordering of MTI can be effectively modeled with a Heisenberg Hamiltonian

$$\mathcal{H}_{\text{spin}} = -\frac{1}{2} \sum_{\langle ij \rangle} J \mathbf{S}_{\text{loc}}^i \cdot \mathbf{S}_{\text{loc}}^j - K \sum_i (S_{\text{loc}}^{i,z})^2. \quad (2)$$

This Hamiltonian includes Heisenberg interaction terms  $J$  for spins at neighboring locations  $i$  and  $j$ , and a magnetic anisotropy parameter  $K$  [64, 65]. The spin operators in terms of Holstein-Primakoff (HP) transformation are given by

$$S_{\text{loc}}^{i,+} \approx \sqrt{2s} b_i^\dagger, \quad S_{\text{loc}}^{i,-} \approx \sqrt{2s} b_i, \quad S_{\text{loc}}^{i,z} = s - b_i^\dagger b_i. \quad (3)$$

Utilizing the HP transformation, we obtain the dispersion relation of magnons (spin waves) in the system as

$$\mathcal{H}_m = \sum_{\mathbf{q}} \omega_{\mathbf{q}} b_{\mathbf{q}}^\dagger b_{\mathbf{q}}, \quad (4)$$

with the effective low-energy dispersion relations  $\omega_{\mathbf{q}} = \Delta + D|\mathbf{q}|^2$  and  $\omega_{\mathbf{q}} = \sqrt{\Delta + D|\mathbf{q}|^2}$  in the FM and AFM phases, respectively [66–68]. Assuming a square lattice, the gaps and dispersion coefficients for the FM and AFM cases are given by

$$\Delta = \begin{cases} 2sK, & \text{(FM)} \\ 4s^2K(K+4J), & \text{(AFM)} \end{cases} \quad (5)$$

$$D = \begin{cases} 2sJa_0^2, & \text{(FM)} \\ 2sJ^2a_0^2, & \text{(AFM)} \end{cases} \quad (6)$$

where  $s$  represents a spin of local moments as in HP transformation, and  $a_0$  denotes the lattice spacing [68, 69]. Note the different physical units of  $D$  and  $\Delta$  for the FM and AFM cases [70].

There exists an  $sd$  exchange coupling between itinerant electrons of the surface states and the local moments. This coupling can generally be expressed as

$$\mathcal{H}_{\text{sd}} = \sum_{\mathbf{q}} \mathbf{s}_{\mathbf{q}} \cdot \mathbb{J}_{\text{sd}} \cdot \mathbf{S}_{\text{loc}}(-\mathbf{q}), \quad (7)$$

where the itinerant electrons' spin density operator is given by  $\mathbf{s}_{\mathbf{q}} = \sum_{\mathbf{k}} \psi_{\mathbf{k}}^{\dagger} \boldsymbol{\sigma} \psi_{\mathbf{k}+\mathbf{q}}$ . Here,  $\mathbb{J}_{sd}$  denotes the matrix of coupling strength, with components

$$\mathbb{J}_{sd} = \begin{pmatrix} \mathbb{J}_{sd}^{xx} & \mathbb{J}_{sd}^{xy} \\ \mathbb{J}_{sd}^{yx} & \mathbb{J}_{sd}^{yy} \end{pmatrix}, \quad (8)$$

assuming a magnetization along the  $z$  direction and neglecting the component of magnons parallel to the magnetization [71]. In general, the full  $3 \times 3$  matrix  $\mathbb{J}_{sd}$  can be decomposed into an isotropic Heisenberg, a Dzyaloshinskii-Moriya (DM), and an anisotropic Ising term, as shown in Ref. [72]. Substituting the result of the HP transformation for local spins in the  $sd$  Hamiltonian, we obtain the electron-magnon interactions

$$\mathcal{H}_{em} = \sum_{\mathbf{q}} g_{em} (\mathbf{s}_{\mathbf{q}} \cdot \hat{\mathbf{n}} b_{\mathbf{q}}^{\dagger} + \mathbf{s}_{-\mathbf{q}} \cdot \hat{\mathbf{n}}^* b_{-\mathbf{q}}), \quad (9)$$

where the electron-magnon coupling strength is given by  $g_{em} = |\mathbb{J}_{sd}|$ , determined by the determinant of the  $sd$  coupling matrix. In the coordinate system where magnetization is aligned along  $z$ , the complex unit vector  $\hat{\mathbf{n}}$  is expressed as

$$\hat{\mathbf{n}} = \frac{1}{|\mathbb{J}_{sd}|} [(\mathbb{J}_{sd}^{xx} + i \mathbb{J}_{sd}^{xy}) \hat{\mathbf{x}} + (\mathbb{J}_{sd}^{yx} + i \mathbb{J}_{sd}^{yy}) \hat{\mathbf{y}}]. \quad (10)$$

In special cases when the  $sd$  exchange consists of either isotropic Heisenberg, anti-symmetric (DM), symmetric (Kitaev), or Ising types, the unit vector has a simple expression as summarized in the following:

$$\hat{\mathbf{n}} = \begin{cases} \hat{\mathbf{x}} + i \hat{\mathbf{y}} & \text{Heisenberg} \\ \hat{\mathbf{y}} - i \hat{\mathbf{x}} & \text{anti-symmetric (DM)} \\ \hat{\mathbf{y}} + i \hat{\mathbf{x}} & \text{symmetric (Kitaev-like)} \\ \hat{\mathbf{x}} \text{ or } \hat{\mathbf{y}} & \text{Ising} \end{cases}. \quad (11)$$

Combining all elements, the complete Hamiltonian of the surface states coupled to magnetic excitations is given by  $\mathcal{H} = \mathcal{H}_e + \mathcal{H}_m + \mathcal{H}_{em}$ .

**Magnon-mediated fermionic interactions.** By treating the electron-magnon couplings perturbatively, a well-justified approach in realistic magnetic materials, we can integrate out the magnon part of the Hamiltonian, resulting in effective interactions among electrons. This process, schematically illustrated in Fig. 2, can be mathematically executed using the canonical transformation method, as shown in Supplementary Materials [73]. In the low-temperature limit, where magnetic excitations are nearly frozen, the effective interaction between surface states electrons is obtained as

$$\mathcal{H}_{int} \approx -\frac{1}{2} \sum_{\mathbf{q}} \frac{g_{em}^2}{\omega_{\mathbf{q}}} \sum_{\mu\nu} n_{\mu} n_{\nu} s_{\mathbf{q}}^{\mu} s_{-\mathbf{q}}^{\nu}. \quad (12)$$

The matrix structure of this interaction is rich, offering a versatile situation where different forms of interaction can be acquired by manipulating the details of the underlying electron-magnon coupling, which may vary with the types of magnetic materials and their orderings.

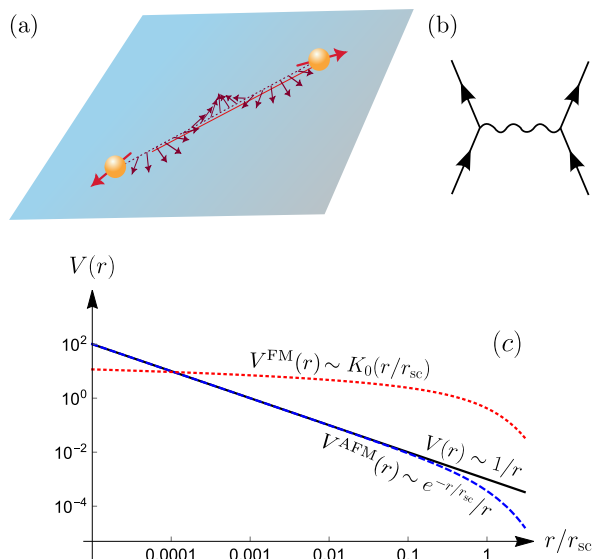


FIG. 2. Magnon-mediated interaction between itinerant electrons within surface states (a) The schematic depiction illustrating how magnons can mediate an effective (possibly long-range) interaction among surface-state electrons. (b) A corresponding Feynman diagram is presented, featuring straight arrows indicating the electron propagator and a wiggly line representing the magnon propagator. (c) The profile of the magnon-mediated interaction potential  $V(r)$ , is depicted on a log-log scale against the interparticle distance  $r$ . The comparison includes FM (dotted red curve) and AFM (dashed blue curve) systems, juxtaposed with the standard Coulomb potential  $V(r) \sim 1/r$ . The effective screening length is expressed as  $r_{sc} = \sqrt{D/\Delta}$ . The numerical values along the  $y$ -axis are presented in arbitrary units.

In general, electron-magnon coupling can have some momentum dependence as  $g_{\mathbf{q}}$ , which is disregarded here when starting from a short-range  $sd$  coupling as the underlying mechanism of electron-magnon interaction. Now, due to the magnon dispersion, the resulting fermionic interaction matrix element in Eq. (12) becomes  $V_q^{FM} = g_{em}^2/(\Delta + Dq^2)$  and  $V_q^{AFM} = g_{em}^2/(\Delta + Dq^2)^{1/2}$  for FM and AFM cases, respectively. The more interesting result is for FM system which despite its resemblance to a screened Coulomb interaction in three spatial dimensions, it significantly differs from a Coulomb-like interaction as it acts between essentially 2D electrons. The real-space form of this interaction is given by the modified Bessel function of the second kind  $V^{FM}(r) = V_0 K_0(r/r_{sc})$ , with  $V_0 = g_{em}^2/(2\pi D)$  and an effective screening length  $r_{sc} = \sqrt{D/\Delta}$  determined by the magnon gap. Beyond this length, the potential  $V^{FM}(r)$  exponentially decays. Unlike the ordinary Coulomb interaction, where the screening parameter is determined by the electronic density of states (DOS) at the Fermi level, here the effective screening is controlled by the magnonic gap  $\Delta$  and is completely independent of DOS. In the limit of a vanishingly small magnon gap, the screening

length diverges, and the interaction becomes long-range with very weak logarithmic dependence. The resulting long-range effective interaction between electrons when the magnons are gapless, asymptotically approaches an infinite-range interaction, resembling the exactly-solvable model of Hatsugai and Kohmoto [56]. In AFM case though, as we have shown in Supplementary Materials [73], the real space form of the interaction turns out to be identical to fully screened Yukawa type form  $V^{\text{AFM}}(r) \propto e^{-r/r_{sc}}/r$  for which we do not expect a radically interesting renormalization effects on the dispersion of topological surface states. This is in part understandable from the fact that due to the difference in their low-energy dispersion relations, FM magnons density of states are typically much higher than AFM case.

Here, our main focus is on the limit of unscreened or weakly screened effective interaction as it is possible in FM case, which will be discussed next. But before that, let us highlight the basic features of the opposite limit, characterized by a large magnon gap leading to an almost flat dispersion  $\omega_q \sim \text{cte}$  for magnons. In this case, the effective interaction is strongly screened, acquiring a momentum-independent coupling constant and giving rise to a short-range interaction. The resulting full Hamiltonian in this limit resembles the Thirring model, a simplistic quantum field theory for interacting fermions [74, 75]. Moreover, it constitutes a special case of the *Gross-Neveu model*, first introduced as a toy model in quantum chromodynamics. This model has recently regained interest, particularly within the condensed matter community [76–86]. The connection to the Gross-Neveu model [87] becomes more profound when dealing with situations with more than one Dirac cone, a typical scenario in Weyl/Dirac materials. Indeed, the role of magnon-induced interactions in magnetic Weyl and Dirac semimetals is an interesting problem on its own, which will be studied elsewhere.

**Interaction effect on surface states.** We are now prepared to investigate the influence of the interactions given by Eq. (12) on the dispersion of topological surface states. In the weak coupling limit, the primary effect of interactions is represented by the self-energy at the one-loop approximation, given by

$$\Sigma(\mathbf{k}) = \boldsymbol{\sigma} \cdot \hat{\mathbf{n}} \Xi(\mathbf{k}) \boldsymbol{\sigma} \cdot \hat{\mathbf{n}}^*. \quad (13)$$

Here,  $\Xi(\mathbf{k})$  is defined as

$$\Xi(\mathbf{k}) = - \sum_{\mathbf{k}'} \frac{g_{\text{em}}^2}{\omega_{\mathbf{k}-\mathbf{k}'}} i \int \frac{d\omega}{2\pi} \mathbf{G}(\mathbf{k}', i\omega), \quad (14)$$

which corresponds to the exchange contribution [59, 88]. The bare Green's function  $\mathbf{G}(\mathbf{k}, i\omega)$  of the surface states is obtained from the Hamiltonian (1) and is given by

$$\mathbf{G}(\mathbf{k}, i\omega) = - \frac{i\omega + v_F \mathbf{k} \cdot \boldsymbol{\sigma} + m_{\perp} \sigma_{\perp}}{\omega^2 + v_F^2 |\mathbf{k}|^2 + m_{\perp}^2}. \quad (15)$$

As detailed in the Supplementary Materials [73], we can precisely derive the self-energy expression

$$\Xi(\mathbf{k}) = -f_3(\tilde{k}) v_F \mathbf{k} \cdot \boldsymbol{\sigma} - f_1(\tilde{k}) m_{\perp} \sigma_{\perp}. \quad (16)$$

Here, the momentum-dependent renormalization functions are given by the expression (the graphical illustration of  $f_n$  functions are given in [73])

$$f_n(\tilde{k}) = \int_0^1 \frac{dx}{4\pi} \frac{x^{n/2} (1-x)^{-1/2}}{\sqrt{x\alpha^2 + x(1-x)\tilde{k}^2 + (1-x)\tilde{m}_{\perp}^2}}, \quad (17)$$

which depends on the momentum, as well as the magnon and electron gaps. Please note that  $\tilde{k} = k/k_{\text{o}}$  and  $\tilde{m}_{\perp} = m_{\perp}/(v_F k_{\text{o}})$  are scaled with  $k_{\text{o}} = [g_{\text{em}}^2/(v_F D)]^{1/3}$  denoting a momentum scale at which electrons kinetic energy  $v_F k$  and the interaction energy scale induced by magnons  $g_{\text{em}}^2/(Dk^2)$  become equal. Consequently, the parameter  $\alpha = 1/(k_{\text{o}} r_{\text{sc}}) = \sqrt{\Delta/D}/k_{\text{o}} = \Delta^{1/2} D^{-1/6} v_F^{1/3} g_{\text{em}}^{-2/3}$  denotes the dimensionless scale of the screening length  $r_{\text{sc}}$  or equivalently, the magnon gap  $\Delta$ .

## DISCUSSION

Since the self-energies are purely real, there is no level broadening, and the corresponding many-body effects only yield a renormalization of the energy dispersion, given by  $\varepsilon_{\mathbf{k},\pm} = \text{diag}[\mathcal{H}_e(\mathbf{k}) + \Sigma(\mathbf{k})]$ . The self-energy, as given by Eq. (16), results in three distinct manifestations of band renormalization effects whose strengths determined by the functions  $f_{1,3}(\tilde{k})$ . First, there is gap renormalization, characterized by the term proportional to  $m_{\perp} \sigma_z$  for top or bottom surfaces. The second effect is momentum-dependent velocity renormalization, which itself divides into isotropic and anisotropic velocity renormalization, as discussed below. Interestingly, due to the spin-dependent matrix structure of the effective interactions (12), and considering that only the top surface has a Dirac gap  $m_{\perp}$  in the non-interacting limit, the gap and velocity renormalization effects are only present for the top and side surfaces, respectively. Finally, we can also have a momentum-dependent tilting of Dirac cone as we will see later on.

Let us first consider the side surfaces where, due to the absence of a Dirac gap in the noninteracting limit, only the first term of Eq. (16) is relevant to them. In the cases of isotropic Heisenberg-, DM-, and Kitaev-type electron-magnon couplings, the self-energy corrections are expressed as

$$\Sigma_{\text{aniso}}(k_x, k_z)|_{\text{side}} = f_3(\tilde{k}) v_F k_z (\pm \sigma_0 + \sigma_z), \quad (18)$$

where the  $'-'$  sign applies for the Kitaev-type coupling and the  $'+'$  for the two others. This implies that solely the  $z$ -component of velocity within one of the two dispersion branches undergoes renormalization, leading to a combination of velocity change and *tilting* effects associated to  $\sigma_z$  and  $\sigma_0$  terms, respectively. These features

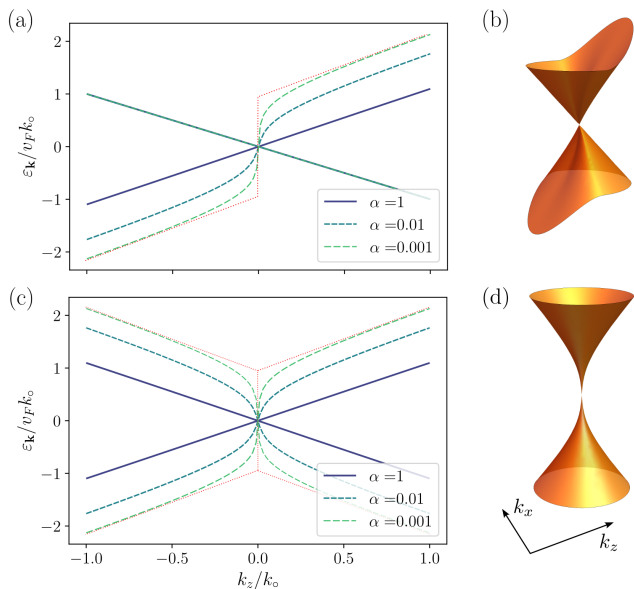


FIG. 3. Interaction-induced changes in the dispersion relation at the vicinity of Dirac point for side surfaces. (a) and (b) show the spectrum for anisotropic case caused by the self-energy corrections in Eq. (18), while (c) and (d) correspond to the isotropic case governed by the self-energy in Eq. (19). In (b) and (d) we have set  $\alpha = 0.01$  with  $\alpha$  being related to the magnon gap. The velocity renormalization in the vicinity of Dirac point further increases by decreasing  $\alpha$  and asymptotically diverges for  $\alpha \rightarrow 0$ . Red dotted lines in (a) and (c) are shown as eye-guide to illustrate the connection to massless-like gap opening.

are shown in Fig. 3(a), illustrating the effective band dispersion with respect to momentum  $k_z$  when  $k_x = 0$ . Consequently, the complete dispersion as a function of both momenta ( $k_z, k_x$ ) unveils a remarkably intriguing anisotropic spectrum, as demonstrated in Fig. 3(b).

Interestingly, with a distinctly anisotropic Ising-type electron-magnon coupling, denoted by  $\hat{\mathbf{n}}_{\text{I}} = \hat{\mathbf{y}}$  for the side surface in the  $xz$  plane, an entirely isotropic self-energy given by

$$\Sigma_{\text{iso}}(k_x, k_z)|_{\text{side}} = f_3(\tilde{k}) v_F \mathbf{k} \cdot \boldsymbol{\sigma} \quad (19)$$

emerges, which gives rise to an isotropic velocity renormalization. The modified dispersion relations are illustrated in Fig. 3(c) and (d) for surface states at the side surfaces, assuming the Ising form for electron-magnon coupling. The results clearly indicate that the most significant changes in the dispersion occur in the vicinity of momenta  $kr_{\text{sc}} \lesssim 1$ , with the strength of renormalization dictated by the dimensionless parameter  $\alpha = 1/(k_o r_{\text{sc}})$ . This is evident when considering the small momentum limit  $k \rightarrow 0$  in the presence of a finite screening length  $r_{\text{sc}}$ , which results in a normalized velocity

$$\frac{v_*}{v_F} = 1 + (3\pi\alpha)^{-1} \quad (20)$$

by taking the small momentum limit of the renormalization function  $f_3(\tilde{k} \rightarrow 0) \rightarrow 1/(3\pi\alpha)$ . The impact of the many-body interaction is weak or moderate when  $\alpha \lesssim 1$ , corresponding to a short-range interaction potential with relatively small  $r_{\text{sc}}$ .

However, the normalized velocity grows linearly with  $r_{\text{sc}}$  and, notably, diverges in the limit of an infinitely large screening length ( $r_{\text{sc}} \rightarrow \infty$  or equivalently  $\alpha \rightarrow 0$ ). This limit can be also understood by considering a finite nonzero momentum and first taking the limit  $\alpha \rightarrow 0$  of the renormalization function  $f_3$ , which is found to be  $\lim_{\alpha \rightarrow 0} f_3 = Ik_o/k$  with  $I = \int_0^1 \frac{dx}{4\pi} x(1-x)^{-1}$  being a singular integral. Assuming a regularised value of integral  $I$  implies that  $f_3 \mathbf{k} \cdot \boldsymbol{\sigma} \rightarrow Ik_o \tilde{\mathbf{k}} \cdot \boldsymbol{\sigma}$  which resembles massless gap term [59]. This scenario aligns with the previously mentioned Hatsugai-Kohmoto (HK) physics, resulting in the appearance of a rigid shift of Dirac cones in opposite directions in energy as depicted by dotted red lines in Fig. 3(a) and (c).

Now, we turn to the surfaces in the  $xy$  plane perpendicular to the magnetization, for which the self-energy becomes

$$\Sigma(k_x, k_y)|_{\text{top}} = f_1(\tilde{k}) m_z (\pm \sigma_0 + \sigma_z), \quad (21)$$

for the three forms of electron-magnon coupling matrix. Note that  $m_{\perp}$  has been we have substituted with  $m_z$  for the surfaces parallel to the  $xy$  plane. In Eq. (21), the '+' sign corresponds to the isotropic Heisenberg and DM cases, while the '-' sign corresponds to the Kitaev-type form of electron-magnon coupling. Remember that the polarization vectors for the above three cases are given by  $\hat{\mathbf{n}}_H = \hat{\mathbf{x}} + i\hat{\mathbf{y}}$  and  $\hat{\mathbf{n}}_{\text{DM}} = \hat{\mathbf{y}} - i\hat{\mathbf{x}}$ , respectively. By plugging Eq. (16) into Eq. (14) for the two polarization vectors, we can easily obtain the self-energy (21). Subsequently, for surface states in the  $xy$  planes, we find that the main effects are a renormalized Dirac gap  $m_* = m_z [1 + f_1(\tilde{k})]$  and a constant shift in energy. In the vicinity of the Dirac point  $\mathbf{k} = 0$ , we find that  $f_1(\mathbf{k} = 0) \rightarrow 1/(2\pi\alpha)$  and  $f_1(\mathbf{k} = 0) \rightarrow 1/(2\pi\tilde{m}_z) \ln(\tilde{m}_z/\alpha)$  for the regimes of relatively small noninteracting gap ( $\tilde{m}_z \ll \alpha$ ) and large gap ( $\tilde{m}_z \gg \alpha$ ), respectively. Hence, the renormalized gap for these two cases read

$$\frac{m_*}{m_z} \approx \begin{cases} 1 + \frac{1}{2\pi\alpha}, & m_z \ll v_F k_o \alpha \\ 1 + \frac{v_F k_o}{2\pi m_z} \ln\left(\frac{m_z}{v_F k_o \alpha}\right), & m_z \gg v_F k_o \alpha \end{cases} \quad (22)$$

This result indicates that as the magnon gap decreases, which also reduces  $\alpha$ , the renormalization becomes more significant in both of the limits above. On one hand, when the bare electronic gap and the magnon gap simultaneously approaches zero (i.e.  $\alpha \sim \tilde{m}_z \rightarrow 0$ ), we can expect a regime where  $m_* = m_z/(2\pi\alpha)$  remains finite. This implies an interaction-induced gap-opening that requires a spontaneous breaking of the time-reversal symmetry. On the other hand, when the bare Dirac gap is large ( $m_z \gg v_F k_o \alpha$ ), the renormalization effects show a logarithmic dependence  $\ln(m_z/v_F k_o \alpha) \equiv \ln(m_z r_{\text{sc}}/v_F)$

which diverges in the limit of  $r_{sc} \rightarrow \infty$  corresponding to gapless magnons. This logarithmic divergence arises from the strong infrared feature of the effective interaction coupling matrix element  $g_{em}^2/\omega_{\mathbf{q}}$  in the absence of a magnon gap. Therefore, it suggests that the massive Dirac liquid is prone to instabilities in the presence of these strong interactions, which warrants separate investigation in future studies.

**Relevance to real materials.** We have seen that magnons can mediate effective interactions among electrons with quite different behavior in FM and AFM TIs. While in FM case we have a strong Coulomb-like interaction which approaches an infinite-range for gapless magnons at the level of one-loop self-energy, for AFM we always get a highly screened Yukawa type interactions. This readily can suggest that different forms of magnon dispersion and subsequently the effective magnon-mediated interactions for the two different magnetic ordering can potentially be another source for the differences in their surface states.

One of the most studied MTIs is stoichiometric  $\text{MnBi}_2\text{Te}_4$  with an *A*-type AFM ordering, where local moments are ferromagnetically aligned in the perpendicular direction within the Mn planes but antiferromagnetically ordered between adjacent layers. For this type of MTIs, as an approximation, we can assume that magnons contributing to the top/bottom surfaces are more like FM magnons, while for the side surfaces, AFM magnons have the major contribution. This means that in  $\text{MnBi}_2\text{Te}_4$ , only the surfaces perpendicular to the magnetic ordering are significantly influenced by the magnon-mediated interaction effects studied here, since effective interactions due to the AFM magnons are much weaker. In contrast, our results for the side surface states are mostly relevant in fully ferromagnetically-ordered MTIs, such as  $\text{MnBi}_8\text{Te}_{13}$ . In particular, MTIs with FM order, in which magnetic anisotropy is weak or absent and thus have a small magnon gap, are the best candidates to experimentally explore our predictions for many-body effects associated with magnons on the topological surface states.

As mentioned earlier, due to the long-range nature of the magnon-mediate interactions for gapless magnons, the leading order self-energy calculation here coincides with the exact result for the case of infinite-range (HK) interaction [56, 59, 60, 89]. This consistency at the one-loop self-energy level, underscores the depth of the observed renormalization effects. Notably, the one-loop approximation utilized in this analysis approaches the accuracy of the infinite-range scenario, effectively governing the comprehensive many-body aspects, as demonstrated in prior investigations [59–61]. Consequently, the pro-

found renormalization of the dispersion relation induced by long-range magnon-mediated interactions should, at least in essence, persist in a more involved many-body analysis beyond one-loop approximation. A more careful study employing a renormalization group formulation can further substantiate this physical insight, akin to analogous studies conducted on Coulomb interactions in graphene [82, 90].

It should be mentioned that direct Coulomb electron-electron interactions and the associated screening or anti-screening due to many-body effects have been neglected in our analysis. However, our main findings remain qualitatively unchanged even when considering these Coulomb interaction effects. This persistence is due to the singularity of the magnon-mediated interaction at the long-wavelength limit, which cannot be eliminated by Coulomb screening effects. Additionally, we emphasize that our focus in this study is on the zero-temperature limit. This choice is justified by the low critical temperatures of most MTI materials, rendering finite-temperature effects negligible.

**Conclusions.** In summary, we have found that magnon-mediated interactions play a crucial role in determining many-body effects on the dispersion relation of surface states in magnetic topological insulators. Specifically, we demonstrate that ferromagnetic magnons can induce strong fermionic interactions, making magnetic topological insulators promising systems for exploring intriguing yet elusive many-body effects. Notably, we observe gap enhancements and Fermi velocity divergences resembling spectra with massless-like gap openings on the top and side surfaces of ferromagnetic topological insulators (see Fig. 1).

Our findings regarding the coupling between surface electrons and bulk magnons offer insights into the electronic properties of topological surface states and may shed light on current discrepancies in photoemission spectroscopy of surface states. Furthermore, by exploring various methods for modifying the electronic dispersion of surface states, our findings can be applied to engineer spintronic applications of magnetic topological insulators, leveraging the interaction between magnons and electrons.

**Acknowledgement.** The authors acknowledge Emanuele Cappelluti for helpful discussions. HR acknowledges the support of Swedish Research Council (VR Starting Grant No. 2018-04252). AGM acknowledges financial support from Jane and Aatos Erkkö Foundation.

- 
- [1] M. Z. Hasan and C. L. Kane, “Colloquium: Topological insulators,” *Rev. Mod. Phys.* **82**, 3045–3067 (2010).  
 [2] Xiao-Liang Qi and Shou-Cheng Zhang, “Topological in-

- ulators and superconductors,” *Rev. Mod. Phys.* **83**, 1057–1110 (2011).  
 [3] Yoichi Ando, “Topological insulator materials,” *Journal*

- of the Physical Society of Japan **82**, 102001 (2013).
- [4] Oliver Breunig and Yoichi Ando, “Opportunities in topological insulator devices,” *Nature Reviews Physics* **4**, 184 (2022).
  - [5] Tomoki Ozawa, Hannah M. Price, Alberto Amo, Nathan Goldman, Mohammad Hafezi, Ling Lu, Mikael C. Rechtsman, David Schuster, Jonathan Simon, Oded Zilberberg, and Iacopo Carusotto, “Topological photonics,” *Rev. Mod. Phys.* **91**, 015006 (2019).
  - [6] Chetan Nayak, Steven H. Simon, Ady Stern, Michael Freedman, and Sankar Das Sarma, “Non-Abelian anyons and topological quantum computation,” *Rev. Mod. Phys.* **80**, 1083–1159 (2008).
  - [7] Joel E Moore, “The birth of topological insulators,” *Nature* **464**, 194 (2010).
  - [8] Yasuhiro Hatsugai, “Chern number and edge states in the integer quantum hall effect,” *Phys. Rev. Lett.* **71**, 3697–3700 (1993).
  - [9] Gian Michele Graf and Marcello Porta, “Bulk-edge correspondence for two-dimensional topological insulators,” *Commun. Math. Phys.* **324**, 851 (2013).
  - [10] Emil Prodan and Hermann Schulz-Baldes, *Bulk and boundary invariants for complex topological insulators* (Springer, Cham, 2016).
  - [11] Yoshinori Tokura, Kenji Yasuda, and Atsushi Tsukazaki, “Magnetic topological insulators,” *Nature Reviews Physics* **1**, 126–143 (2019).
  - [12] Ferhat Katmis, Valeria Lauter, Flavio S Nogueira, Badih A Assaf, Michelle E Jamer, Peng Wei, Biswarup Satpati, John W Freeland, Ilya Eremin, Don Heiman, *et al.*, “A high-temperature ferromagnetic topological insulating phase by proximity coupling,” *Nature* **533**, 513–516 (2016).
  - [13] V Bonbien, Fengjun Zhuo, A Salimath, O Ly, A About, and A Manchon, “Topological aspects of antiferromagnets,” *J. Phys. D: Appl. Phys.* **55**, 103002 (2021).
  - [14] Roger S. K. Mong, Andrew M. Essin, and Joel E. Moore, “Antiferromagnetic topological insulators,” *Phys. Rev. B* **81**, 245209 (2010).
  - [15] Nicodemos Varnava and David Vanderbilt, “Surfaces of axion insulators,” *Phys. Rev. B* **98**, 245117 (2018).
  - [16] Dongqin Zhang, Minji Shi, Tongshuai Zhu, Dingyu Xing, Haijun Zhang, and Jing Wang, “Topological axion states in the magnetic insulator  $\text{mnbi}_2\text{te}_4$  with the quantized magnetoelectric effect,” *Phys. Rev. Lett.* **122**, 206401 (2019).
  - [17] Di Xiao, Jue Jiang, Jae-Ho Shin, Wenbo Wang, Fei Wang, Yi-Fan Zhao, Chaoxing Liu, Weida Wu, Moses H. W. Chan, Nitin Samarth, and Cui-Zu Chang, “Realization of the Axion Insulator State in Quantum Anomalous Hall Sandwich Heterostructures,” *Phys. Rev. Lett.* **120**, 056801 (2018).
  - [18] Chang Liu, Yongchao Wang, Hao Li, Yang Wu, Yaoxin Li, Jiaheng Li, Ke He, Yong Xu, Jinsong Zhang, and Yayu Wang, “Robust axion insulator and Chern insulator phases in a two-dimensional antiferromagnetic topological insulator,” *Nat. Mater.* **19**, 522–527 (2020).
  - [19] Akihiko Sekine and Kentaro Nomura, “Axion electrodynamics in topological materials,” *Journal of Applied Physics* **129**, 141101 (2021).
  - [20] Libor Šmejkal, Yuriy Mokrousov, Binghai Yan, and Allan H MacDonald, “Topological antiferromagnetic spintronics,” *Nat. Phys.* **14**, 242 (2018).
  - [21] Dennis M Nenzo, Christina AC Garcia, Johannes Gooth, Claudia Felser, and Prineha Narang, “Axion physics in condensed-matter systems,” *Nature Reviews Physics* **2**, 682–696 (2020).
  - [22] AR Mellnik, JS Lee, A Richardella, JL Grab, PJ Mintun, Mark H Fischer, Abolhassan Vaezi, Aurelien Manchon, E-A Kim, Nitin Samarth, *et al.*, “Spin-transfer torque generated by a topological insulator,” *Nature* **511**, 449 (2014).
  - [23] Qing Lin He, Xufeng Kou, Alexander J Grutter, Gen Yin, Lei Pan, Xiaoyu Che, Yuxiang Liu, Tianxiao Nie, Bin Zhang, Steven M Disseler, *et al.*, “Tailoring exchange couplings in magnetic topological-insulator/antiferromagnet heterostructures,” *Nat. Mater.* **16**, 94 (2017).
  - [24] Ali G. Moghaddam, Alireza Qaiumzadeh, Anna Dyrdał, and Jamal Berakdar, “Highly tunable spin-orbit torque and anisotropic magnetoresistance in a topological insulator thin film attached to ferromagnetic layer,” *Phys. Rev. Lett.* **125**, 196801 (2020).
  - [25] Qing Lin He, Taylor L Hughes, N Peter Armitage, Yoshinori Tokura, and Kang L Wang, “Topological spintronics and magnetoelectronics,” *Nat. Mat.* **21**, 15 (2022).
  - [26] Mikhail M Otrokov, Ilya I Klimovskikh, Hendrik Bentmann, D Estyunin, Alexander Zeugner, Ziya S Aliev, S Gaß, AUB Wolter, AV Koroleva, Alexander M Shikin, *et al.*, “Prediction and observation of an antiferromagnetic topological insulator,” *Nature* **576**, 416 (2019).
  - [27] R. C. Vidal, H. Bentmann, T. R. F. Peixoto, A. Zeugner, S. Moser, C.-H. Min, S. Schatz, K. Kifner, M. Ünzelmann, C. I. Fornari, H. B. Vasili, M. Valvidares, K. Sakamoto, D. Mondal, J. Fujii, I. Vobornik, S. Jung, C. Cacho, T. K. Kim, R. J. Koch, C. Jozwiak, A. Bostwick, J. D. Denlinger, E. Rotenberg, J. Buck, M. Hoesch, F. Diekmann, S. Rohlf, M. Kalläne, K. Rossnagel, M. M. Otrokov, E. V. Chulkov, M. Ruck, A. Isaeva, and F. Reinert, “Surface states and Rashba-type spin polarization in antiferromagnetic  $\text{MnBi}_2\text{Te}_4(0001)$ ,” *Phys. Rev. B* **100**, 121104 (2019).
  - [28] Yu-Jie Hao, Pengfei Liu, Yue Feng, Xiao-Ming Ma, Eike F. Schwier, Masashi Arita, Shiv Kumar, Chaowei Hu, Rui’e Lu, Meng Zeng, Yuan Wang, Zhanyang Hao, Hong-Yi Sun, Ke Zhang, Jiawei Mei, Ni Ni, Liusuo Wu, Kenya Shimada, Chaoyu Chen, Qihang Liu, and Chang Liu, “Gapless Surface Dirac Cone in Antiferromagnetic Topological Insulator  $\text{MnBi}_2\text{Te}_4$ ,” *Phys. Rev. X* **9**, 041038 (2019).
  - [29] Hang Li, Shun-Ye Gao, Shao-Feng Duan, Yuan-Feng Xu, Ke-Jia Zhu, Shang-Jie Tian, Jia-Cheng Gao, Wen-Hui Fan, Zhi-Cheng Rao, Jie-Rui Huang, Jia-Jun Li, Da-Yu Yan, Zheng-Tai Liu, Wan-Ling Liu, Yao-Bo Huang, Yu-Liang Li, Yi Liu, Guo-Bin Zhang, Peng Zhang, Takeshi Kondo, Shik Shin, He-Chang Lei, You-Guo Shi, Wen-Tao Zhang, Hong-Ming Weng, Tian Qian, and Hong Ding, “Dirac Surface States in Intrinsic Magnetic Topological Insulators  $\text{EuSn}_2\text{As}_2$  and  $\text{MnBi}_{2n}\text{Te}_{3n+1}$ ,” *Phys. Rev. X* **9**, 041039 (2019).
  - [30] Y. J. Chen, L. X. Xu, J. H. Li, Y. W. Li, H. Y. Wang, C. F. Zhang, H. Li, Y. Wu, A. J. Liang, C. Chen, S. W. Jung, C. Cacho, Y. H. Mao, S. Liu, M. X. Wang, Y. F. Guo, Y. Xu, Z. K. Liu, L. X. Yang, and Y. L. Chen, “Topological Electronic Structure and Its Temperature Evolution in Antiferromagnetic Topological Insulator  $\text{MnBi}_2\text{Te}_4$ ,” *Phys. Rev. X* **9**, 041040 (2019).

- [31] Jiazhen Wu, Fucai Liu, Masato Sasase, Koichiro Ienaga, Yukiko Obata, Ryu Yukawa, Koji Horiba, Hiroshi Kumigashira, Satoshi Okuma, Takeshi Inoshita, and Hideo Hosono, “Natural van der Waals heterostructural single crystals with both magnetic and topological properties,” *Sci. Adv.* **5**, eaax9989 (2019).
- [32] Raphael C. Vidal, Alexander Zeugner, Jorge I. Facio, Rajyavardhan Ray, M. Hossein Haghghi, Anja U. B. Wolter, Laura T. Corredor Bohorquez, Federico Cagliaris, Simon Moser, Tim Figgemeier, Thiago R. F. Peixoto, Hari Babu Vasili, Manuel Valvidares, Sungwon Jung, Cephise Cacho, Alexey Alfonsov, Kavita Mehlatat, Vladislav Kataev, Christian Hess, Manuel Richter, Bernd Büchner, Jeroen van den Brink, Michael Ruck, Friedrich Reinert, Hendrik Bentmann, and Anna Isaeva, “Topological Electronic Structure and Intrinsic Magnetization in  $\text{MnBi}_4\text{Te}_7$ : A  $\text{Bi}_2\text{Te}_3$  Derivative with a Periodic Mn Sublattice,” *Phys. Rev. X* **9**, 041065 (2019).
- [33] Chaowei Hu, Kyle N Gordon, Pengfei Liu, Jinyu Liu, Xiaoping Zhou, Peipei Hao, Dushyant Narayan, Eve Emmanouilidou, Hongyi Sun, Yuntian Liu, *et al.*, “A van der Waals antiferromagnetic topological insulator with weak interlayer magnetic coupling,” *Nat. Commun.* **11**, 1–8 (2020).
- [34] Przemyslaw Swatek, Yun Wu, Lin-Lin Wang, Kyungchan Lee, Benjamin Schruck, Jiaqiang Yan, and Adam Kaminski, “Gapless Dirac surface states in the antiferromagnetic topological insulator  $\text{MnBi}_2\text{Te}_4$ ,” *Phys. Rev. B* **101**, 161109 (2020).
- [35] Yong Hu, Lixuan Xu, Mengzhu Shi, Aiyun Luo, Shuting Peng, Z. Y. Wang, J. J. Ying, T. Wu, Z. K. Liu, C. F. Zhang, Y. L. Chen, G. Xu, X.-H. Chen, and J.-F. He, “Universal gapless Dirac cone and tunable topological states in  $(\text{MnBi}_2\text{Te}_4)_m(\text{Bi}_2\text{Te}_3)_n$  heterostructures,” *Phys. Rev. B* **101**, 161113 (2020).
- [36] Kyle N Gordon, Hongyi Sun, Chaowei Hu, A Garrison Linn, Haoxiang Li, Yuntian Liu, Pengfei Liu, Scott Mackey, Qihang Liu, Ni Ni, *et al.*, “Strongly Gapped Topological Surface States on Protected Surfaces of Antiferromagnetic  $\text{MnBi}_4\text{Te}_7$  and  $\text{MnBi}_6\text{Te}_{10}$ ,” [arXiv:1910.13943](https://arxiv.org/abs/1910.13943) (2019).
- [37] Xiao-Ming Ma, Zhongjia Chen, Eike F. Schwier, Yang Zhang, Yu-Jie Hao, Shiv Kumar, Ruie Lu, Jifeng Shao, Yuanjun Jin, Meng Zeng, Xiang-Rui Liu, Zhanyang Hao, Ke Zhang, Wumiti Mansuer, Chunyao Song, Yuan Wang, Boyan Zhao, Cai Liu, Ke Deng, Jiawei Mei, Kenya Shimada, Yue Zhao, Xingjiang Zhou, Bing Shen, Wen Huang, Chang Liu, Hu Xu, and Chaoyu Chen, “Hybridization-induced gapped and gapless states on the surface of magnetic topological insulators,” *Phys. Rev. B* **102**, 245136 (2020).
- [38] Ilya I. Klimovskikh, Mikhail M. Otrokov, Dmitry Estyunin, Sergey V. Ereemeev, Sergey O. Filnov, Alexandra Koroleva, Eugene Shevchenko, Vladimir Voroshnin, Artem G. Rybkin, Igor P. Rusinov, Maria Blanco-Rey, Martin Hoffmann, Ziya S. Aliev, Mahammad B. Babanly, Imamaddin R. Amiraslanov, Nadir A. Abdullayev, Vladimir N. Zverev, Akio Kimura, Oleg E. Tereshchenko, Konstantin A. Kokh, Luca Petaccia, Giovanni Di Santo, Arthur Ernst, Pedro M. Echenique, Nazim T. Mamedov, Alexander M. Shikin, and Eugene V. Chulkov, “Tunable 3D/2D magnetism in the  $(\text{MnBi}_2\text{Te}_4)(\text{Bi}_2\text{Te}_3)_m$  topological insulators family,” *npj Quantum Mater.* **5**, 54 (2020).
- [39] LX Xu, YH Mao, HY Wang, JH Li, YJ Chen, YY Xia, YW Li, J Zhang, HJ Zheng, K Huang, *et al.*, “Persistent gapless surface states in  $\text{MnBi}_2\text{Te}_4/\text{Bi}_2\text{Te}_3$  superlattice antiferromagnetic topological insulator,” [arXiv:1910.11014](https://arxiv.org/abs/1910.11014) (2019).
- [40] Xuefeng Wu, Jiayu Li, Xiao-Ming Ma, Yu Zhang, Yuntian Liu, Chun-Sheng Zhou, Jifeng Shao, Qiaoming Wang, Yu-Jie Hao, Yue Feng, Eike F. Schwier, Shiv Kumar, Hongyi Sun, Pengfei Liu, Kenya Shimada, Koji Miyamoto, Taichi Okuda, Kedong Wang, Maohai Xie, Chaoyu Chen, Qihang Liu, Chang Liu, and Yue Zhao, “Distinct topological surface states on the two terminations of  $\text{MnBi}_4\text{Te}_7$ ,” *Phys. Rev. X* **10**, 031013 (2020).
- [41] Yufei Zhao and Qihang Liu, “Routes to realize the axion-insulator phase in  $\text{mnbi}_2\text{te}_4(\text{bi}_2\text{te}_3)_n$  family,” *Appl. Phys. Lett.* **119**, 060502 (2021).
- [42] R. C. Vidal, H. Bentmann, J. I. Facio, T. Heider, P. Kagerer, C. I. Fornari, T. R. F. Peixoto, T. Figgemeier, S. Jung, C. Cacho, B. Büchner, J. van den Brink, C. M. Schneider, L. Plucinski, E. F. Schwier, K. Shimada, M. Richter, A. Isaeva, and F. Reinert, “Orbital Complexity in Intrinsic Magnetic Topological Insulators  $\text{MnBi}_4\text{Te}_7$  and  $\text{MnBi}_6\text{Te}_{10}$ ,” *Phys. Rev. Lett.* **126**, 176403 (2021).
- [43] Chaowei Hu, Lei Ding, Kyle N Gordon, Barun Ghosh, Hung-Ju Tien, Haoxiang Li, A Garrison Linn, Shang-Wei Lien, Cheng-Yi Huang, Scott Mackey, *et al.*, “Realization of an intrinsic ferromagnetic topological state in  $\text{MnBi}_8\text{Te}_{13}$ ,” *Sci. Adv.* **6**, eaba4275 (2020).
- [44] AM Shikin, DA Estyunin, NL Zaitsev, D Glazkova, II Klimovskikh, S Filnov, AG Rybkin, EF Schwier, S Kumar, A Kimura, *et al.*, “Sample-dependent Dirac point gap in  $\text{MnBi}_2\text{Te}_4$  and its response to the applied surface charge: a combined photoemission and ab initio study,” [arXiv:2107.04428](https://arxiv.org/abs/2107.04428) (2021).
- [45] A. Alfonsov, J. I. Facio, K. Mehlatat, A. G. Moghaddam, R. Ray, A. Zeugner, M. Richter, J. van den Brink, A. Isaeva, B. Büchner, and V. Kataev, “Strongly anisotropic spin dynamics in magnetic topological insulators,” *Phys. Rev. B* **103**, L180403 (2021).
- [46] Gabriele Naselli, Ali G. Moghaddam, Solange Di Napoli, Veronica Vildosola, Ion Cosma Fulga, Jeroen van den Brink, and Jorge I. Facio, “Magnetic warping in topological insulators,” [arXiv:2205.09218](https://arxiv.org/abs/2205.09218) (2022).
- [47] Ruie Lu, Hongyi Sun, Shiv Kumar, Yuan Wang, Mingqiang Gu, Meng Zeng, Yu-Jie Hao, Jiayu Li, Jifeng Shao, Xiao-Ming Ma, Zhanyang Hao, Ke Zhang, Wumiti Mansuer, Jiawei Mei, Yue Zhao, Cai Liu, Ke Deng, Wen Huang, Bing Shen, Kenya Shimada, Eike F. Schwier, Chang Liu, Qihang Liu, and Chaoyu Chen, “Half-magnetic topological insulator with magnetization-induced dirac gap at a selected surface,” *Phys. Rev. X* **11**, 011039 (2021).
- [48] Stefan Wimmer, Jaime Sánchez-Barriga, Philipp Küppers, Andreas Ney, Enrico Schierle, Friedrich Freyse, Ondrej Caha, Jan Michalička, Marcus Liebmann, Daniel Primetzhofer, Martin Hoffman, Arthur Ernst, Mikhail M. Otrokov, Gustav Bihlmayer, Eugen Weschke, Bella Lake, Evgueni V. Chulkov, Markus Morgenstern, Günther Bauer, Gunther Springholz, and Oliver Rader, “Mn-rich  $\text{mnsb}_2\text{te}_4$ : A topological insulator with magnetic gap closing at high curie temperatures of 45–50 k,” *Advanced Materials* **33**, 2102935 (2021).
- [49] Qile Li, Chi Xuan Trang, Weikang Wu, Jinwoong

- Hwang, David Cortie, Nikhil Medhekar, Sung-Kwan Mo, Shengyuan A. Yang, and Mark T. Edmonds, “Large magnetic gap in a designer ferromagnet–topological insulator–ferromagnet heterostructure,” *Advanced Materials* **34**, 2107520 (2022).
- [50] Mengke Liu, Chao Lei, Hyunsue Kim, Yanxing Li, Lisa Frammolino, Jiaqiang Yan, Allan H. Macdonald, and Chih-Kang Shih, “Visualizing the interplay of dirac mass gap and magnetism at nanoscale in intrinsic magnetic topological insulators,” *Proceedings of the National Academy of Sciences* **119**, e2207681119 (2022).
- [51] Kristian Mæland, Håkon I. Røst, Justin W. Wells, and Asle Sudbø, “Electron-magnon coupling and quasiparticle lifetimes on the surface of a topological insulator,” *Phys. Rev. B* **104**, 125125 (2021).
- [52] Marius Scholten, Jorge I. Facio, Rajyavardhan Ray, Ilya M. Eremin, Jeroen van den Brink, and Flavio S. Nogueira, “Finite temperature fluctuation-induced order and responses in magnetic topological insulators,” *Phys. Rev. Research* **3**, L032014 (2021).
- [53] David J. Gross and André Neveu, “Dynamical symmetry breaking in asymptotically free field theories,” *Phys. Rev. D* **10**, 3235 (1974).
- [54] J. Zinn-Justin, “Four-fermion interaction near four dimensions,” *Nuclear Physics B* **367**, 105 (1991).
- [55] Moshe Moshe and Jean Zinn-Justin, “Quantum field theory in the large  $n$  limit: a review,” *Physics Reports* **385**, 69 (2003).
- [56] Yasuhiro Hatsugai and Mahito Kohmoto, “Exactly solvable model of correlated lattice electrons in any dimensions,” *Journal of the Physical Society of Japan* **61**, 2056–2069 (1992).
- [57] L. Benfatto and E. Cappelluti, “Spectroscopic signatures of massless gap opening in graphene,” *Phys. Rev. B* **78**, 115434 (2008).
- [58] Emmanuele Cappelluti, Lara Benfatto, Marco Papagno, Daniela Pacilè, Polina M. Sheverdyaeva, and Paolo Moras, “Massless dirac cones in graphene: Experiments and theory,” *Annalen der Physik* **526**, 387 (2014).
- [59] Habib Rostami, Emmanuele Cappelluti, and Alexander V. Balatsky, “Helical metals and insulators: Sheet singularity of the inflated berry monopole,” *Phys. Rev. B* **98**, 245114 (2018).
- [60] Takahiro Morimoto and Naoto Nagaosa, “Weyl mott insulator,” *Scientific reports* **6**, 1–6 (2016).
- [61] Tobias Meng and Jan Carl Budich, “Unpaired weyl nodes from long-ranged interactions: Fate of quantum anomalies,” *Phys. Rev. Lett.* **122**, 046402 (2019).
- [62] Philip W. Phillips, Luke Yeo, and Edwin W. Huang, “Exact theory for superconductivity in a doped mott insulator,” *Nature Physics* **16**, 1175–1180 (2020).
- [63] Peizhi Mai, Jinchao Zhao, Gaurav Tenkila, Nico A. Hacker, Dhruv Kush, Derek Pan, and Philip W. Phillips, “New approach to strong correlation: Twisting hubbard into the orbital hatsugai-kohmoto model,” (2024), [arXiv:2401.08746 \[cond-mat.str-el\]](https://arxiv.org/abs/2401.08746).
- [64] T. Holstein and H. Primakoff, “Field dependence of the intrinsic domain magnetization of a ferromagnet,” *Phys. Rev.* **58**, 1098–1113 (1940).
- [65] Øyvind Johansen, Akashdeep Kamra, Camilo Ulloa, Arne Brataas, and Rembert A. Duine, “Magnon-mediated indirect exciton condensation through antiferromagnetic insulators,” *Phys. Rev. Lett.* **123**, 167203 (2019).
- [66] Charles Kittel, *Quantum theory of solids* (Wiley, New York, 1963).
- [67] Anil Prabhakar and Daniel D Stancil, *Spin waves: Theory and applications*, Vol. 5 (Springer, 2009).
- [68] Eirik Erlandsen, Akashdeep Kamra, Arne Brataas, and Asle Sudbø, “Enhancement of superconductivity mediated by antiferromagnetic squeezed magnons,” *Phys. Rev. B* **100**, 100503 (2019).
- [69] Eirik Erlandsen, Arne Brataas, and Asle Sudbø, “Magnon-mediated superconductivity on the surface of a topological insulator,” *Phys. Rev. B* **101**, 094503 (2020).
- [70] The reason of this choice, which will be clear later, is to define a single form for the screening length.
- [71] This approximation is equivalent to ignoring the finite magnon population, justified at low temperatures,  $\langle b_q^\dagger b_q \rangle \approx 0$ .
- [72] Changsong Xu, Junsheng Feng, Sergei Prokhorenko, Youstra Nahas, Hongjun Xiang, and L. Bellaiche, “Topological spin texture in janus monolayers of the chromium trihalides  $\text{Cr}(X)_3$ ,” *Phys. Rev. B* **101**, 060404 (2020).
- [73] The details of evaluating integrals over energy and momentum which yields the given final result are shown in the Supplemental Materials.
- [74] Walter E Thirring, “A soluble relativistic field theory,” *Annals of Physics* **3**, 91–112 (1958).
- [75] J. Ignacio Cirac, Paolo Maraner, and Jiannis K. Pachos, “Cold atom simulation of interacting relativistic quantum field theories,” *Phys. Rev. Lett.* **105**, 190403 (2010).
- [76] Oliver Schnetz, Michael Thies, and Konrad Urlichs, “Phase diagram of the Gross–Neveu model: exact results and condensed matter precursors,” *Annals of Physics* **314**, 425 (2004).
- [77] Igor F. Herbut, “Interactions and phase transitions on graphene’s honeycomb lattice,” *Phys. Rev. Lett.* **97**, 146401 (2006).
- [78] Lukas Janssen and Igor F. Herbut, “Antiferromagnetic critical point on graphene’s honeycomb lattice: A functional renormalization group approach,” *Phys. Rev. B* **89**, 205403 (2014).
- [79] Yuichi Otsuka, Seiji Yunoki, and Sandro Sorella, “Universal quantum criticality in the metal-insulator transition of two-dimensional interacting dirac electrons,” *Phys. Rev. X* **6**, 011029 (2016).
- [80] Nikolai Zerf, Luminita N. Mihaila, Peter Marquard, Igor F. Herbut, and Michael M. Scherer, “Four-loop critical exponents for the gross-neveu-yukawa models,” *Phys. Rev. D* **96**, 096010 (2017).
- [81] Thomas C. Lang and Andreas M. Läuchli, “Quantum monte carlo simulation of the chiral heisenberg gross-neveu-yukawa phase transition with a single dirac cone,” *Phys. Rev. Lett.* **123**, 137602 (2019).
- [82] Ho-Kin Tang, J. N. Leaw, J. N. B. Rodrigues, I. F. Herbut, P. Sengupta, F. F. Assaad, and S. Adam, “The role of electron-electron interactions in two-dimensional dirac fermions,” *Science* **361**, 570 (2018).
- [83] Yi-Zhuang You, Yin-Chen He, Cenke Xu, and Ashvin Vishwanath, “Symmetric fermion mass generation as deconfined quantum criticality,” *Phys. Rev. X* **8**, 011026 (2018).
- [84] Shao-Kai Jian, Shuai Yin, and Brian Swingle, “Universal prethermal dynamics in gross-neveu-yukawa criticality,” *Phys. Rev. Lett.* **123**, 170606 (2019).
- [85] Yoni BenTov, “Fermion masses without symmetry breaking in two spacetime dimensions,” *J. High Energy Phys.*

- [2015](#), [34](#) (2015).
- [86] J. A. Gracey, “Large  $n$  critical exponents for the chiral heisenberg gross-neveu universality class,” [Phys. Rev. D](#) **97**, [105009](#) (2018).
- [87] More precisely, the so-called chiral Heisenberg Gross-Neveu model with the Lagrangian  $\mathcal{L} = i\bar{\psi}_i\partial\psi_i + g^2(\bar{\psi}_i\boldsymbol{\sigma}\psi)_i \cdot (\bar{\psi}_i\boldsymbol{\sigma}\psi_i)$  (see, e.g., [86]).
- [88] Gerald D Mahan, *Many-particle physics* (Springer Science & Business Media, 2013).
- [89] F. S. Nogueira and E. V. Anda, “Study on a toy model of strongly correlated electrons,” *International Journal Of Modern Physics B* **10**, 3705–3716 (1996).
- [90] Hiroki Isobe and Naoto Nagaosa, “Coulomb interaction effect in weyl fermions with tilted energy dispersion in two dimensions,” [Phys. Rev. Lett.](#) **116**, [116803](#) (2016).

# Supplemental Materials: Fate of surface gaps in magnetic topological insulators

Habib Rostami<sup>1</sup> and Ali G. Moghaddam<sup>2,3,4</sup>

<sup>1</sup>*Department of Physics, University of Bath, Claverton Down, Bath BA2 7AY, United Kingdom*

<sup>2</sup>*Department of Physics, Institute for Advanced Studies in Basic Sciences (IASBS), Zanjan 45137-66731, Iran*

<sup>3</sup>*Computational Physics Laboratory, Physics Unit, Faculty of Engineering and Natural Sciences, Tampere University, P.O. Box 692, FI-33014 Tampere, Finland*

<sup>4</sup>*Helsinki Institute of Physics, FI-00014 University of Helsinki, Finland*

(Dated: April 30, 2024)

In the supplementary materials, we provide detailed calculations that are not presented in the main text. The supplementary material is organized into three sections. In the first section, we derive the form of magnon-mediated interactions using the canonical transformation technique. Subsequently, we obtain the explicit form of interactions in real space induced by low-energy magnons in both ferromagnetic and antiferromagnetic settings. In the antiferromagnetic case, we observe a strongly screened form of interaction, while in a ferromagnetic system, interactions can be unscreened when the magnon gap becomes very small. Finally, we present comprehensive calculations for the electronic self-energy due to magnon-mediated interactions in the ferromagnetic case, where many-body effects are more pronounced.

## I. DERIVATION OF MAGNON-MEDIATED INTERACTIONS

We begin by considering a generic relation of canonical transformation in a perturbative way, which reads

$$\tilde{\mathcal{H}} = e^{\mathcal{O}} \mathcal{H} e^{-\mathcal{O}} = \mathcal{H} + [\mathcal{O}, \mathcal{H}] + \frac{1}{2} [\mathcal{O}, [\mathcal{O}, \mathcal{H}]] + \dots \quad (1)$$

to find an effective electron-electron (e-e) interactions mediated by magnons. To this end and in the spirit of Schrieffer-Wolff transformations, we require  $\mathcal{H}_{\text{em}} + [\mathcal{O}, \mathcal{H}_m] = 0$  which is fulfilled by the operator

$$\mathcal{O} = \sum_{\mathbf{q}} \frac{g_{\mathbf{q}}}{\omega_{\mathbf{q}}} (\mathbf{s}_{\mathbf{q}} \cdot \hat{\mathbf{n}} b_{\mathbf{q}}^{\dagger} - \mathbf{s}_{\mathbf{q}} \cdot \hat{\mathbf{n}}^* b_{-\mathbf{q}}). \quad (2)$$

Then, considering the terms up to second-order in the electron-magnon coupling  $g_{\mathbf{q}}$ , we find an effective Hamiltonian for the fermionic part as

$$\mathcal{H}_{\text{eff}} = \tilde{\mathcal{H}}_e + \frac{1}{2} [\mathcal{O}, \mathcal{H}_{\text{em}}], \quad (3)$$

with  $\tilde{\mathcal{H}}_e = \mathcal{H}_e + [\mathcal{O}, \mathcal{H}_e] + \dots$ , which we approximate with  $\mathcal{H}_e$  as it will be justified in what follows. We can easily check that the first correction term  $[\mathcal{O}, \mathcal{H}_e]$  is found to consists of the following expression:

$$\sum_{\mathbf{k}, \mathbf{q}} \frac{g_{\mathbf{q}}}{\omega_{\mathbf{q}}} \psi_{\mathbf{k}}^{\dagger} [\boldsymbol{\sigma} \cdot \hat{\mathbf{n}}, \mathbf{k} \cdot \boldsymbol{\sigma}] \psi_{\mathbf{k}+\mathbf{q}} b_{\mathbf{q}}^{\dagger} + h.c., \quad (4)$$

which is nothing but a correction to the electron-magnon coupling but with effective coupling constant  $g_{\mathbf{q}} v_F k / \omega_{\mathbf{q}}$ . Therefore, assuming small bandwidth  $\Omega$  for electronic surface states and a large magnon gap which arguably represent the physically relevant situation in realistic materials, we always have  $v_F k / \omega_{\mathbf{q}} \ll 1$ , thus we can safely neglect this corrections to the electron-magnon interactions. Likewise by neglecting the next correction terms (or effectively assuming a mere renormalization of coupling constants due to these terms), we rely on the approximation  $\tilde{\mathcal{H}}_e \approx \mathcal{H}_e$  from now on. The second term in the effective Hamiltonian Eq. (3) is found as

$$\frac{1}{2} [\mathcal{O}, \mathcal{H}_{\text{em}}] = \frac{1}{2} \sum_{\mathbf{q}} \frac{g_{\mathbf{q}}^2}{\omega_{\mathbf{q}}} \left( - \{ \mathbf{s}_{\mathbf{q}} \cdot \hat{\mathbf{n}}, \mathbf{s}_{-\mathbf{q}} \cdot \hat{\mathbf{n}}^* \} + 2 [\mathbf{s}_{\mathbf{q}} \cdot \hat{\mathbf{n}}, \mathbf{s}_{\mathbf{q}} \cdot \hat{\mathbf{n}}^*] b_{\mathbf{q}}^{\dagger} b_{-\mathbf{q}} \right), \quad (5)$$

whose first term includes a fermionic interaction whereas the second term yields a renormalization of the fermionic single-particle terms weighted by the magnons population  $\langle b^{\dagger} b \rangle$  [1]. In low-temperature limit where magnon excitations

are almost frozen, only the first term in above expression survives which results in an effective interaction between surface states electrons

$$\mathcal{H}_{\text{int}} \approx -\frac{1}{2} \sum_{\mathbf{q}} \frac{g_{\mathbf{q}}^2}{\omega_{\mathbf{q}}} \{\mathbf{s}_{\mathbf{q}} \cdot \hat{\mathbf{n}}, \mathbf{s}_{-\mathbf{q}} \cdot \hat{\mathbf{n}}^*\}. \quad (6)$$

So that the effective interaction is given as follows

$$V_{\mathbf{q}} = \frac{g_{\mathbf{q}}^2}{\omega_{\mathbf{q}}}. \quad (7)$$

## II. EFFECTIVE INTERACTIONS IN REAL-SPACE

In this part we explore the form of magnon-mediated interactions in real space for both ferromagnetic and antiferromagnetic cases. For FM magnons using the low-energy dispersion relation  $\omega_q = \Delta + Dq^2 = D(r_{\text{sc}}^{-2} + q^2)$  with  $r_{\text{sc}} = \sqrt{D/\Delta}$  and considering short-range electron magnon coupling with a constant momentum-independent coefficient  $g_q = g_{\text{em}}$ , we have

$$\begin{aligned} V(\mathbf{r}) &= \frac{g_{\text{em}}^2}{D} \int \frac{e^{-i\mathbf{q}\cdot\mathbf{r}}}{r_{\text{sc}}^{-2} + q^2} \frac{d^2\mathbf{q}}{(2\pi)^2} = \frac{g_{\text{em}}^2}{D\Gamma(1)} \int_0^\infty d\tau \int e^{-i\mathbf{q}\cdot\mathbf{r}} e^{-\tau(r_{\text{sc}}^{-2} + q^2)} \frac{d^2\mathbf{q}}{(2\pi)^2} \\ &= \frac{g_{\text{em}}^2}{D} \int_0^\infty d\tau e^{-\tau r_{\text{sc}}^{-2}} \int e^{-\tau q^2 - i\mathbf{q}\cdot\mathbf{r}} \frac{d^2\mathbf{q}}{(2\pi)^2} \\ &= \frac{g_{\text{em}}^2}{D} \int_0^\infty d\tau e^{-\tau r_{\text{sc}}^{-2}} \frac{\pi\tau^{-1}}{(2\pi)^2} e^{-\frac{r^2}{4\tau}} \\ &= \frac{g_{\text{em}}^2}{4\pi D} \int_0^\infty d\tau \tau^{-1} e^{-\tau r_{\text{sc}}^{-2}} e^{-\frac{r^2}{4\tau}} \end{aligned} \quad (8)$$

Performing last integral over  $\tau$  gives the Bessel function  $K_0(x)$ . Therefore

$$V(\mathbf{r}) = \frac{g_{\text{em}}^2}{2\pi D} K_0(r/r_{\text{sc}}) \quad (9)$$

We can also obtain the asymptotic behaviors of this interaction in small and large distances;

$$V(\mathbf{r}) = \begin{cases} \frac{g_{\text{em}}^2}{2\pi D} \{\ln(2) - \gamma - \ln(r/r_{\text{sc}}) + \dots\}, & r/r_{\text{sc}} \ll 1 \\ \frac{g_{\text{em}}^2}{2D\sqrt{2\pi}} \frac{e^{-r/r_{\text{sc}}}}{\sqrt{r/r_{\text{sc}}}} + \dots, & r/r_{\text{sc}} \gg 1 \end{cases} \quad (10)$$

The special case of  $\alpha = 0$  can be obtained explicitly as

$$\int_0^\infty d\tau \tau^{-1} e^{-\frac{r^2}{4\tau}} = \int_0^\infty dt t^{-1} e^{-t\frac{r^2}{4}} = \frac{1}{\Gamma(0)} \left(\frac{4}{r^2}\right)^0, \quad (11)$$

corresponding to infinite range interactions.

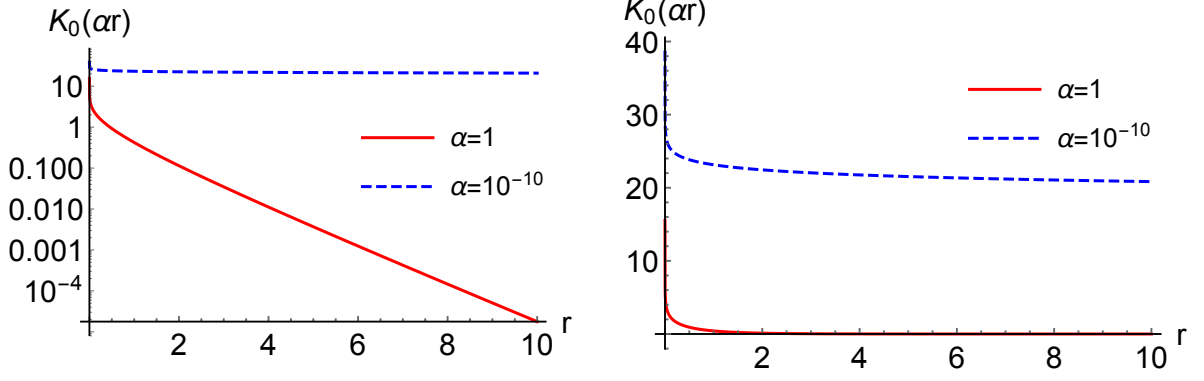


FIG. 1. left: log scale. right: linear scale. As seen for small  $\alpha \rightarrow 0$  we can approximate  $V(r)$  as a constant potential in finite range of  $r$ .

### A. Antiferromagnetic case

For the antiferromagnetic we have  $\omega_{\mathbf{q}} = \sqrt{\Delta + Dq^2} = D^{1/2} \sqrt{r_{sc}^{-2} + q^2}$  leading to

$$\begin{aligned}
 V(\mathbf{r}) &= \frac{g_{em}^2}{\sqrt{D}} \int \frac{e^{-i\mathbf{q}\cdot\mathbf{r}}}{(r_{sc}^{-2} + q^2)^{1/2}} \frac{d^2\mathbf{q}}{(2\pi)^2} = \frac{g_{em}^2}{\sqrt{D}\Gamma(1/2)} \int_0^\infty d\tau \tau^{-1/2} \int e^{-i\mathbf{q}\cdot\mathbf{r}} e^{-\tau(r_{sc}^{-2} + q^2)} \frac{d^2\mathbf{q}}{(2\pi)^2} \\
 &= \frac{g_{em}^2}{\sqrt{D}\Gamma(1/2)} \int_0^\infty d\tau \tau^{-1/2} e^{-\tau r_{sc}^{-2}} \int e^{-\tau q^2 - i\mathbf{q}\cdot\mathbf{r}} \frac{d^2\mathbf{q}}{(2\pi)^2} \\
 &= \frac{g_{em}^2}{\sqrt{D}\Gamma(1/2)} \int_0^\infty d\tau \tau^{-1/2} e^{-\tau r_{sc}^{-2}} \frac{\pi \tau^{-1}}{(2\pi)^2} e^{-\frac{r^2}{4\tau}} \\
 &= \frac{g_{em}^2}{4\pi\sqrt{D}\Gamma(1/2)} \int_0^\infty d\tau \tau^{-3/2} e^{-\tau r_{sc}^{-2}} e^{-\frac{r^2}{4\tau}} = \left( \frac{g_{em}^2}{2\pi\sqrt{D}r_{sc}} \right) \frac{e^{-r/r_{sc}}}{r/r_{sc}} \quad (12)
 \end{aligned}$$

Therefore, for the case AF we obtain a screened inter-particle Coulomb interaction.

### III. SELF-ENERGY CORRECTIONS

In the short-range electron-magnon coupling limit where we have  $g_{\mathbf{q}} = g_{em}$  (subscript  $s$  is used to indicate short range) independent of  $\mathbf{q}$ , the self-energy is given by

$$\Sigma(\mathbf{k}) = \boldsymbol{\sigma} \cdot \hat{\mathbf{n}} \Xi \boldsymbol{\sigma} \cdot \hat{\mathbf{n}}^*, \quad (13)$$

$$\Xi = - \sum_{\mathbf{k}'} \frac{g_s^2}{\Delta + D|\mathbf{k} - \mathbf{k}'|^2} i \int \frac{d\omega}{2\pi} \mathbf{G}_0(\mathbf{k}', i\omega). \quad (14)$$

First, we note that the integration over frequency  $\omega$ , using the Green's function, Eq. (12) in the main text yields

$$i \int \frac{d\omega}{2\pi} \mathbf{G}_0(\mathbf{k}', i\omega) = \frac{1}{2} \frac{v_F \mathbf{k}' \cdot \boldsymbol{\sigma} + m_z \sigma_z}{\sqrt{v_F^2 |\mathbf{k}'|^2 + m_z^2}}. \quad (15)$$

Therefore,

$$-\Xi = I_1 \frac{g_{em}^2 m_z}{2(v_F k_o) D k_o^2} \sigma_z + I_{2,i} \frac{g_{em}^2 (v_F k_o)}{2(v_F k_o) D k_o^2} \sigma_i = I_1 m_z \sigma_z + I_{2,i} v_F k_o \sigma_i, \quad (16)$$

where we set the characteristic wave vector  $k_o$  such that  $g_{em}^2 / (2v_F k_o D k_o^2) = 1$  corresponding a point in which kinetic energy of electrons  $v_F k$  and the magnon-mediated interaction energy scale  $g_{em}^2 m_z / (2D k_o^2)$  become equal.

We need to solve the following integrals

$$I_1 = \sum_{\mathbf{k}'} \frac{1}{\alpha^2 + |\mathbf{k} - \mathbf{k}'|^2} \frac{1}{\sqrt{|\mathbf{k}'|^2 + m^2}} \quad (17)$$

$$I_{2,i} = \sum_{\mathbf{k}'} \frac{1}{\alpha^2 + |\mathbf{k} - \mathbf{k}'|^2} \frac{k'_i}{\sqrt{|\mathbf{k}'|^2 + m^2}}, \quad (18)$$

in which all parameters and variables are re-scaled in terms of  $k_o$ . In particular, we define dimensionless variables  $m = m_z/(v_F k_o)$  and  $\alpha = \sqrt{\Delta/D} k_o^2 > 0$  where the latter also corresponds to the inverse of the scaled screening length  $\alpha = 1/(k_o r_{sc})$  since  $r_{sc} = \sqrt{D/\Delta}$ . Also, we note that the momentum has been made dimensionless as  $k = q/k_o$ . We recall the Feynman parametrization for arbitrary functions  $h_1$  and  $h_2$

$$\frac{1}{h_1^\alpha h_2^\beta} = \frac{\Gamma(\alpha + \beta)}{\Gamma(\alpha)\Gamma(\beta)} \int_0^1 dx \frac{x^{\alpha-1}(1-x)^{\beta-1}}{[xh_1 + (1-x)h_2]^{\alpha+\beta}}, \quad (19)$$

Note the Euler's Gamma-function  $\Gamma(z) = (z-1)!$ . Let's first check the case of  $I_1$  using the Feynman's integration trick:

$$\begin{aligned} \frac{1}{\alpha^2 + |\mathbf{k} - \mathbf{k}'|^2} \frac{1}{(|\mathbf{k}'|^2 + m^2)^{1/2}} &= \frac{\Gamma(3/2)}{\Gamma(1)\Gamma(1/2)} \int_0^1 dx \frac{x^{1/2}(1-x)^{-1/2}}{\{x[\alpha^2 + |\mathbf{k} - \mathbf{k}'|^2] + (1-x)[|\mathbf{k}'|^2 + m^2]\}^{3/2}} \\ &= \frac{\Gamma(3/2)}{\Gamma(1)\Gamma(1/2)} \int_0^1 dx \frac{x^{1/2}(1-x)^{-1/2}}{\{k'^2 - 2x\mathbf{k} \cdot \mathbf{k}' + S(x)\}^{3/2}} \end{aligned} \quad (20)$$

where  $S(x) = x\alpha^2 + xk^2 + (1-x)m^2$ . We now use the Schwinger's parameterization:

$$\frac{1}{h^\alpha} = \frac{1}{\Gamma(\alpha)} \int_0^\infty d\tau \tau^{\alpha-1} e^{-\tau h}, \quad (21)$$

Using the above trick to convert the integrand into a Gaussian functional form:

$$\frac{1}{\{k'^2 - 2x\mathbf{k} \cdot \mathbf{k}' + S(x)\}^{3/2}} = \frac{1}{\Gamma(3/2)} \int_0^\infty d\tau \tau^{1/2} e^{-\tau[k'^2 - 2x\mathbf{k} \cdot \mathbf{k}' + S(x)]} \quad (22)$$

Therefore, we have

$$\begin{aligned} \int \frac{d^D \mathbf{k}'}{(2\pi)^D} \frac{1}{\alpha^2 + |\mathbf{k} - \mathbf{k}'|^2} \frac{1}{(|\mathbf{k}'|^2 + m^2)^{1/2}} &= \frac{1}{\Gamma(1)\Gamma(1/2)} \int_0^1 dx x^{1/2}(1-x)^{-1/2} \int_0^\infty d\tau \tau^{1/2} e^{-\tau S(x)} \\ &\quad \times \int \frac{d^D \mathbf{k}'}{(2\pi)^D} e^{-\tau[k'^2 - 2x\mathbf{k} \cdot \mathbf{k}']} \end{aligned} \quad (23)$$

It is also good to remind Gaussian integral formula:

$$\int \frac{d^D \mathbf{q}}{(2\pi)^D} e^{-\frac{1}{2} \mathbf{q} \cdot \overleftrightarrow{\mathbf{A}} \cdot \mathbf{q} + \mathbf{J} \cdot \mathbf{q}} = \frac{e^{\frac{1}{2} \mathbf{J} \cdot \overleftrightarrow{\mathbf{A}}^{-1} \cdot \mathbf{J}}}{\sqrt{(2\pi)^D \det(\overleftrightarrow{\mathbf{A}})}}, \quad (24)$$

where  $\overleftrightarrow{\mathbf{A}}$ ,  $\mathbf{J}$ , and  $\mathbf{q}$  are defined in a  $D$ -dimensional space which are

$$\mathbf{J} = 2x\tau\mathbf{k}, \quad \overleftrightarrow{\mathbf{A}} = 2\tau I_D, \quad (25)$$

with  $I_D$  is an identify matrix  $D$  dimensions, in the present case. Therefore, we find

$$\int \frac{d^D \mathbf{k}'}{(2\pi)^D} e^{-\tau[k'^2 - 2x\mathbf{k} \cdot \mathbf{k}']} = \frac{e^{\tau x^2 k^2}}{\sqrt{(2\pi)^D (2\tau)^D}} \quad (26)$$

Accordingly, we can write

$$\begin{aligned} \int \frac{d^D \mathbf{k}'}{(2\pi)^D} \frac{1}{\alpha^2 + |\mathbf{k} - \mathbf{k}'|^2} \frac{1}{(|\mathbf{k}'|^2 + m^2)^{1/2}} &= \frac{1}{2^D \pi^{D/2}} \frac{1}{\Gamma(1)\Gamma(1/2)} \int_0^1 dx x^{1/2}(1-x)^{-1/2} \\ &\quad \times \int_0^\infty d\tau \tau^{(1-D)/2} e^{-\tau[S(x) - x^2 k^2]} \end{aligned} \quad (27)$$

Note that

$$\int_0^\infty d\tau \tau^{(1-D)/2} e^{-\tau[S(x)-x^2k^2]} = \frac{\Gamma((3-D)/2)}{[S(x)-x^2k^2]^{(3-D)/2}} \quad (28)$$

Therefore, we find

$$\begin{aligned} \int \frac{d^D \mathbf{k}'}{(2\pi)^D} \frac{1}{\alpha^2 + |\mathbf{k} - \mathbf{k}'|^2} \frac{1}{(|\mathbf{k}'|^2 + m^2)^{1/2}} &= \frac{\Gamma((3-D)/2)}{2^D \pi^{D/2}} \frac{1}{\Gamma(1)\Gamma(1/2)} \\ &\times \int_0^1 dx \frac{x^{1/2}(1-x)^{-1/2}}{[x\alpha^2 + x(1-x)k^2 + (1-x)m^2]^{(3-D)/2}} \end{aligned} \quad (29)$$

The above integral is regular in two dimensions and therefore, we can safely set  $D = 2$  which gives

$$I_1 = \int \frac{d^2 \mathbf{k}'}{(2\pi)^2} \frac{1}{\alpha^2 + |\mathbf{k} - \mathbf{k}'|^2} \frac{1}{(|\mathbf{k}'|^2 + m^2)^{1/2}} = \frac{1}{4\pi} \int_0^1 dx \frac{x^{1/2}(1-x)^{-1/2}}{[x\alpha^2 + x(1-x)k^2 + (1-x)m^2]^{1/2}} \quad (30)$$

Similarly, we find

$$\begin{aligned} \int \frac{d^D \mathbf{k}'}{(2\pi)^D} k'_i e^{-\tau[k'^2 - 2x\mathbf{k} \cdot \mathbf{k}']} &= \left( \frac{1}{2x\tau} \frac{\partial}{\partial k_i} \right) \int \frac{d^D \mathbf{k}'}{(2\pi)^D} e^{-\tau[k'^2 - 2x\mathbf{k} \cdot \mathbf{k}']} \\ &= \left( \frac{1}{2x\tau} \frac{\partial}{\partial k_i} \right) \frac{e^{\tau x^2 k^2}}{\sqrt{(2\pi)^D (2\tau)^D}} = (xk_i) \frac{e^{\tau x^2 k^2}}{\sqrt{(2\pi)^D (2\tau)^D}} \end{aligned} \quad (31)$$

So that,

$$\begin{aligned} \int \frac{d^D \mathbf{k}'}{(2\pi)^D} \frac{1}{\alpha^2 + |\mathbf{k} - \mathbf{k}'|^2} \frac{k'_i}{(|\mathbf{k}'|^2 + m^2)^{1/2}} &= \frac{1}{2^D \pi^{D/2}} \frac{1}{\Gamma(1)\Gamma(1/2)} \int_0^1 dx x^{1/2}(1-x)^{-1/2} \\ &\times \int_0^\infty d\tau \tau^{(1-D)/2} (xk_i) e^{-\tau[S(x)-x^2k^2]} \end{aligned} \quad (32)$$

Thus,

$$\begin{aligned} \int \frac{d^D \mathbf{k}'}{(2\pi)^D} \frac{1}{\alpha^2 + |\mathbf{k} - \mathbf{k}'|^2} \frac{k'_i}{(|\mathbf{k}'|^2 + m^2)^{1/2}} &= \frac{k_i}{2^D \pi^{D/2}} \frac{1}{\Gamma(1)\Gamma(1/2)} \int_0^1 dx x^{3/2}(1-x)^{-1/2} \\ &\times \int_0^\infty d\tau \tau^{(1-D)/2} e^{-\tau[S(x)-x^2k^2]} \end{aligned} \quad (33)$$

Therefore,

$$\int \frac{d^D \mathbf{k}'}{(2\pi)^D} \frac{1}{\alpha^2 + |\mathbf{k} - \mathbf{k}'|^2} \frac{k'_i}{(|\mathbf{k}'|^2 + m^2)^{1/2}} = \frac{k_i}{2^D \pi^{D/2}} \frac{\Gamma((3-D)/2)}{\Gamma(1)\Gamma(1/2)} \int_0^1 dx \frac{x^{3/2}(1-x)^{-1/2}}{[S(x)-x^2k^2]^{(3-D)/2}} \quad (34)$$

In two dimensions we find

$$I_{2,i} = \int \frac{d^2 \mathbf{k}'}{(2\pi)^2} \frac{1}{\alpha^2 + |\mathbf{k} - \mathbf{k}'|^2} \frac{k'_i}{(|\mathbf{k}'|^2 + m^2)^{1/2}} = \frac{k_i}{4\pi} \int_0^1 dx \frac{x^{3/2}(1-x)^{-1/2}}{[x\alpha^2 + x(1-x)k^2 + (1-x)m^2]^{1/2}} \quad (35)$$

Finally, we find

$$I_1 = \int \frac{d^2 \mathbf{k}'}{(2\pi)^2} \frac{1}{\alpha^2 + |\mathbf{k} - \mathbf{k}'|^2} \frac{1}{(|\mathbf{k}'|^2 + m^2)^{1/2}} = f_1(k, \alpha, m) \quad (36)$$

$$I_2 = \int \frac{d^2 \mathbf{k}'}{(2\pi)^2} \frac{1}{\alpha^2 + |\mathbf{k} - \mathbf{k}'|^2} \frac{\hat{\sigma} \cdot \mathbf{k}'}{(|\mathbf{k}'|^2 + m^2)^{1/2}} = (\hat{\sigma} \cdot \mathbf{k}) f_3(k, \alpha, m) \quad (37)$$

where we define function  $f_n(k, \alpha, m)$ :

$$f_n(k, \alpha, m) = \frac{1}{4\pi} \int_0^1 dx \frac{x^{n/2}(1-x)^{-1/2}}{[x\alpha^2 + x(1-x)k^2 + (1-x)m^2]^{1/2}} = a_n + O(k^2) \quad (38)$$

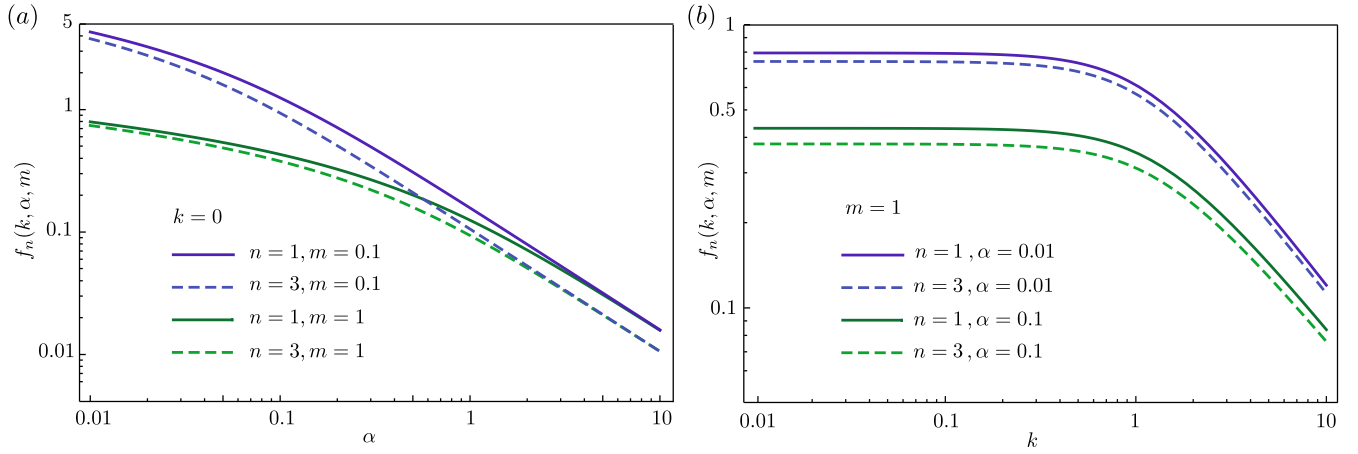


FIG. 2.  $f_1$  and  $f_3$  functions in logarithmic scales versus (a)  $\alpha$  at  $k = 0$ , and (b)  $k$  for  $m = 1$ . For comparison, two different values for  $m$  and  $\alpha$  have been considered in panels (a) and (b), respectively.

Now, we perform the integration over  $x$  for small  $k$  limit:

$$a_1 = \frac{m}{2\pi} \frac{K\left(1 - \frac{\alpha^2}{m^2}\right) - E\left(1 - \frac{\alpha^2}{m^2}\right)}{m^2 - \alpha^2} \quad (39)$$

$$a_3 = \frac{m}{6\pi} \frac{(3m^2 - \alpha^2) K\left(1 - \frac{\alpha^2}{m^2}\right) + 2(\alpha^2 - 2m^2) E\left(1 - \frac{\alpha^2}{m^2}\right)}{(m^2 - \alpha^2)^2} \quad (40)$$

We find the following asymptotic behaviors

$$a_1 \approx \frac{1}{2\pi} \frac{1}{\alpha}, \quad \text{for } \alpha \gg m \quad (41)$$

$$a_1 \approx \frac{1}{2\pi} \frac{\ln(m/\alpha)}{m}, \quad \text{for } \alpha \ll m \quad (42)$$

and

$$a_3 \approx \frac{1}{3\pi} \frac{1}{\alpha}, \quad \text{for } \alpha \gg m \quad (43)$$

$$a_3 \approx \frac{1}{2\pi} \frac{\ln(m/\alpha)}{m}. \quad \text{for } \alpha \ll m \quad (44)$$

We conclude this section by expressing the self-energy part  $\Xi$ , as given in Eq. (16), through the substitution of Eqs. (36) and (37). The resulting form is presented as

$$\Xi = -f_3(k, \alpha, m)v_F \mathbf{k} \cdot \boldsymbol{\sigma} - f_1(k, \alpha, m)m_z \sigma_z, \quad (45)$$

which agrees with the form presented in the main text as Eq. (13).

### A. Self-energy and renormalized energy dispersion of surface states

Here, we elaborate the results for the self-energy  $\Sigma$  in a bit more detail. Let's first concentrate on the case of side surfaces parallel to the magnetization which has gapless surface states. For these surfaces, we see that the influence of self-energy consists of different forms of velocity renormalizations and a tilting term depending on the detailed matrix structure of magnon-electron coupling. Considering four interesting situations of completely isotropic Heisenberg, pure DM term, Kitaev type and highly anisotropic coupling to the magnons, which correspond to  $\mathbf{n}_H = \hat{\mathbf{x}} + i\hat{\mathbf{y}}$ ,

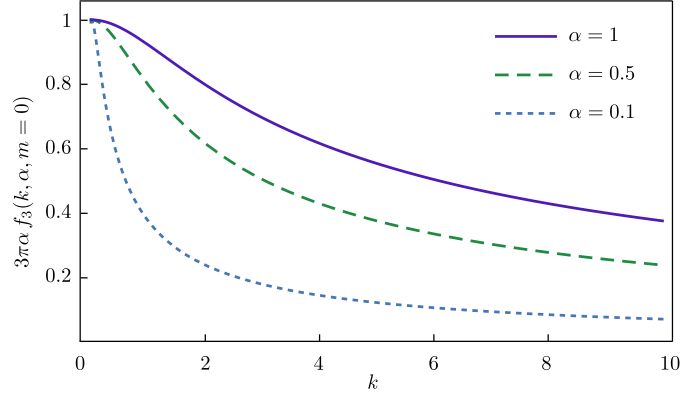


FIG. 3. Momentum dependence of  $f_3(k, \alpha, 0)$

$\mathbf{n}_{DM} = \hat{\mathbf{y}} - i\hat{\mathbf{x}}$ ,  $\mathbf{n}_K = \hat{\mathbf{y}} + i\hat{\mathbf{x}}$ , and  $\mathbf{n}_I = \hat{\mathbf{y}}$ , respectively, we can easily see that

$$\boldsymbol{\Sigma}_H = \boldsymbol{\sigma} \cdot \hat{\mathbf{n}}_H \Xi \boldsymbol{\sigma} \cdot \hat{\mathbf{n}}_H^* = -(\sigma_z + \sigma_0) \Xi_z, \quad (46)$$

$$\boldsymbol{\Sigma}_{DM} = \boldsymbol{\sigma} \cdot \hat{\mathbf{n}}_{DM} \Xi \boldsymbol{\sigma} \cdot \hat{\mathbf{n}}_{DM}^* = -(\sigma_z + \sigma_0) \Xi_z, \quad (47)$$

$$\boldsymbol{\Sigma}_K = \boldsymbol{\sigma} \cdot \hat{\mathbf{n}}_K \Xi \boldsymbol{\sigma} \cdot \hat{\mathbf{n}}_K^* = -(\sigma_z - \sigma_0) \Xi_z, \quad (48)$$

$$\boldsymbol{\Sigma}_I|_{\hat{\mathbf{n}}=\hat{\mathbf{y}}} = \sigma_y \Xi \sigma_y = -\sigma_x \Xi_x - \sigma_z \Xi_z. \quad (49)$$

Therefore, for the side surfaces elongated in  $xz$  plane, the self-energy corrections are

$$\boldsymbol{\Sigma}_{H,DM}(k_x, k_z) = f_3(\sqrt{k_x^2 + k_z^2}, \alpha, 0) v_F k_z (\sigma_z + \sigma_0), \quad (50)$$

$$\boldsymbol{\Sigma}_K(k_x, k_z) = f_3(\sqrt{k_x^2 + k_z^2}, \alpha, 0) v_F k_z (\sigma_z - \sigma_0), \quad (51)$$

$$\boldsymbol{\Sigma}_I(k_x, k_z) = f_3(\sqrt{k_x^2 + k_z^2}, \alpha, 0) v_F (k_x \sigma_x + k_z \sigma_z). \quad (52)$$

In fact, depending on the form of magnon-electron coupling terms, we can have anisotropy besides a Dirac cone tilting, and just an overall isotropic velocity renormalization in the two cases, respectively. The effect of self-energies can be constituted to a dimensionless renormalization factor  $f_3(k, \alpha, 0)$  which has a strong momentum dependence and vanishes in a power-law form for large enough momenta. This can be clearly seen by writing down the explicit form of  $f_3(k, \alpha, 0)$  which reads

$$f_3(k, \alpha, 0) = -\frac{\sqrt{\alpha^2 + k^2}}{4\pi k^2} + \frac{(\alpha^2 + 2k^2)}{4\pi k^3} \ln \left( \frac{\sqrt{\alpha^2 + k^2} + k}{\alpha} \right) \quad (53)$$

As this expression and its illustration in Fig. 3 show, the renormalization becomes negligible for  $k \gg \alpha$ . In addition, its amplitude at very low momenta scales inversely with  $\alpha$  as it is followed from the limiting form of the function  $f_3$  which is given by

$$f_3(k, \alpha, 0) \approx \frac{1}{3\pi\alpha} - \frac{k^2}{30\pi\alpha^3} + O(k^4). \quad (54)$$

An immediate consequence of this result is that when the magnon gap becomes very small ( $\alpha \rightarrow 0$ ), we find a very radical change in the effective velocity of electrons but only in the vicinity of very small  $k \lesssim \alpha$  as it has been illustrated in Fig. 2 (b) and (c) in the main text.

Now, we return to the top surface where we have a magnetic gap  $m_z$  and considering isotropic coupling to the magnons ( $\mathbf{n}_I = \hat{\mathbf{x}} + i\hat{\mathbf{y}}$ ), the matrix structure of interaction only leaves the term proportional  $m_z$  and we have

$$\boldsymbol{\Sigma}_{\text{top}}(k_x, k_y) = m_z f_1(\sqrt{k_x^2 + k_y^2}, \alpha, m_z) (\sigma_z + \sigma_0). \quad (55)$$

where

$$f_1(k, \alpha, m_z) = \frac{1}{2\pi k} \ln \left( \frac{\sqrt{\alpha^2 + k^2} + k}{\alpha} \right) + O(m_z^2) \approx \frac{1}{2\pi\alpha} - \frac{k^2}{12\pi\alpha^3} + O(k^4). \quad (56)$$

When the magnon gap is large enough such that ( $\alpha > m_z \neq 0$ ), the self-energy will modify the band gap by  $m_z/(2\pi\alpha)$ , whereas in the opposite limit of vanishingly small magnon gap for which  $\alpha \ll m_z$ , we find logarithmic correction term  $(1/2\pi) \ln(m_z/\alpha)$  as can be seen from Eq. (42).

---

[1] The fact that the second term represent a single-particle fermionic terms is followed from the commutation relation  $[\mathbf{s}_\mathbf{q} \cdot \hat{\mathbf{n}}, \mathbf{s}_\mathbf{q} \cdot \hat{\mathbf{n}}^*] = i(\hat{\mathbf{n}} \times \hat{\mathbf{n}}^*) \cdot \mathbf{s}_\mathbf{q}$ .